PHYSICAL REVIEW A **87**, 041804(R) (2013)

Self-pulsing nanocavity laser

A. M. Yacomotti,* S. Haddadi, and S. Barbay†
Laboratoire de Photonique et de Nanostructures, LPN-CNRS UPR 20, Route de Nozay, 91460 Marcoussis, France
(Received 9 November 2012; published 30 April 2013; corrected 23 July 2013)

We propose a scheme to achieve controllable self-pulsing operation in a semiconductor photonic-crystal nanolaser. The scheme is based on coupling two asymmetric nanocavities and pumping only one of them. As a result, either periodic or chaotic subnanosecond Q-switched pulses can emerge. A coupled-mode approach is used to model the system and study the bifurcation diagram. An experimental realization is proposed on the basis of two evanescently coupled photonic-crystal nanocavities.

DOI: 10.1103/PhysRevA.87.041804 PACS number(s): 42.65.Sf, 42.55.Tv, 42.60.By, 42.60.Gd

Introduction. Nanolasers are very exciting objects of study since they are believed to be essential building blocks to bridge the gap between electronics and photonics. They may offer extremely small footprints and scalability as key ingredients for future high density integrated optoelectronic circuits. Physically, the small mode and material volumes in play have dramatic consequences on fundamental parameters such as the recombination rates of excited atoms or charge carriers. In this context, ultrafast laser operation has been recently demonstrated in photonic-crystal (PhC) cavities [1–4], with picosecond response times [1] obtained thanks to QED phenomena such as the Purcell effect [5]. Yet, short optical pulses have only been triggered by ultrashort pump pulses. Building up stable self-pulsing (SP) lasers at the nanoscale would be a next step towards the realization of either classic or quantum—i.e., single photon [6,7]—advanced light nanosources.

Self-oscillatory dynamics has been theoretically studied in a variety of nonlinear nanocavity systems [8–10]. In a laser, two main dynamical mechanisms may give rise to SP: multimode instabilities leading to mode locking, and single-mode instabilities in the form of amplitude and/or frequency modulated oscillations. Mode locking relies on somewhat long microcavities supporting several longitudinal laser modes. A mode-locked PhC laser has been numerically investigated in [11], exploiting the large bandwidth of a 20-period, PhC defect cavity and predicting output pulses as short as a few picoseconds. On the contrary, single-mode instabilities can generally be obtained in shorter cavities with, e.g., semiconductor quantum wells as active media, with longer pulse durations. This is due to both the restricted bandwidth of single-mode operation, and to the material relaxation times: 100 ps to 1 ns for carrier recombination in semiconductors, and 100 ns to 1 μs for thermal diffusion. A possible single-mode instability leading to self-pulsation in nanocavities is thermo-optical, regenerative oscillations [12]. It has been reported in L3 PhC nanocavities, made by three missing holes in the Γ-K direction of a triangular PhC, in III-V semiconductors [13] as well as in hybrid graphene-Si membrane devices [14]. In those experiments, pulse durations are governed by thermo-optical switching, usually longer than ~10 ns. Another well-known single-mode instability leading to SP is passive Q switching, which can be obtained with an intracavity saturable absorber [15,16]. Passive Q switching in nanolasers has not been demonstrated so far.

A question then arises: Is it possible to achieve fast (multi-GHz) SP nanolasers? Nanocavity is the answer key: The small mode volume combined with moderate quality factors may lead to high modulation frequencies. In this regard, ultrafast modulated oscillations (up to 130-GHz bandwidth) have been reported in a PhC defect cavity [17], with a saturable absorber given by the residual absorption of the laser mode tails. Although high-frequency oscillations were shown, it has not been confirmed yet whether these PhC nanolasers exhibited self-pulsation or undamped relaxation oscillations. In order to build up robust SP nanolasers, we propose in this Rapid Communication a system based on two coupled asymmetric PhC nanocavities (Fig. 1) that exhibits subnanosecond self-pulsation based on saturable absorption. We show that by controlling the coupling constant between the two nanocavities, a dynamical regime very different from the one usually found in single-mode models for bisection semiconductor lasers can emerge. In particular, the self-pulsing regime in bisection lasers results from strong optical coupling between the pumped and unpumped regions and emerges from global (homoclinic) limit cycle bifurcations. In our coupled-cavity model, self-pulsing is achieved through local (Hopf) bifurcations with a significantly reduced coupling coefficient between the pumped and unpumped cavities. Electromagnetic simulations are performed on a coupled-nanocavity system and relevant parameters are extracted that show the possibility to implement these ideas in a real system.

Model. Let us suppose that the field in each cavity 1,2 is $a_{1,2}$ with frequencies $\omega_{1,2}$. We introduce adimensional rate equations for scaled field amplitudes $A_{1,2}$ in the rotating frame at angular velocity ω_2 and scaled carrier densities $N_{1,2}$ with respect to their transparency values $\tilde{N}_0$ [$N_{1,2} \propto (\tilde{N}/\tilde{N}_0 - 1)$] in each semiconductor nanocavity analogously as in [18]. Coupling of the two cavities is introduced in a coupled-mode approach. The dynamical equations read

$$\begin{aligned}
\frac{dA_1}{dt} &= -A_1 + (1 + i\alpha)A_1N_1 + (i\kappa + \gamma)A_2,\\
\frac{dA_2}{dt} &= (-1 + i\delta)A_2 + (1 + i\alpha)A_2N_2 + (i\kappa + \gamma)A_1, \quad (1)\\
\frac{dN_{1,2}}{dt} &= \gamma_r[g_{1,2} - N_{1,2}(1 + s_{1,2}|A_{1,2}|^2)].
\end{aligned}$$

*alejandro.giacomotti@lpn.cnrs.fr
†sylvain.barbay@lpn.cnrs.fr

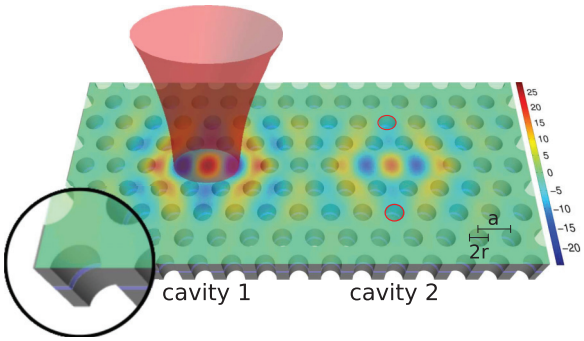

FIG. 1. (Color) Design of the asymmetric, coupled L3 PhC nanocavity laser. The lattice parameter is $a = 435$ nm and the hole radius is $r = 0.3a$. Two hole radii (in red) are modified to adjust the detuning between the cavities. The calculated mode profile is overlayed on the cavity drawing for a modified radius $r' = 1.15r$. The cavity width is 265 nm and an active layer is grown at its center.

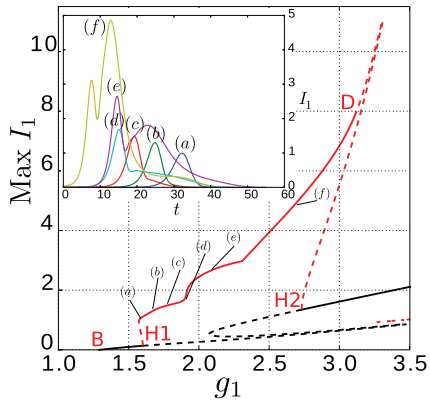

FIG. 2. (Color online) Bifurcation diagram of the set of equations (1): Max(I_1) vs g_1. Continuous line, stable solution; dashed line, unstable solution; dark, cw solution; red (light gray), SP solution. Inset: time trace of the periodic pulses at different pump intensities. Parameters are given in the text.

Time has been rescaled to the mode lifetime τ_c. The nonradiative carrier recombination rate is γ_r, and pumping in each cavity is $g_{1,2} = \Gamma\sigma_{1,2}N_0c\tau_c(P/P_0 - 1)/n$, where Γ is the confinement factor, $\sigma_{1,2}$ is the differential gain or loss, c/n is the group velocity, P is the pumping, and P_0 is the pumping at transparency. The scaled pumping $g_{1,2}$ is positive for a gain medium, negative for an absorptive medium, and zero at transparency. Carrier and thermal diffusion processes are neglected in this model. We disregard bimolecular recombination terms in a first approximation since they are generally negligible with respect to no-radiative recombination as long as we operate close to transparency. The phase-amplitude coupling term α is between 2 and 10 in the case of quantum wells as active material considered here. The nanocavity fields are coupled through an imaginary, energy-conserving term, κ. A real coupling-loss term γ is also included. The saturation parameter $s_{1,2}$ is defined as $s_1 = 1$ and $s_2 = s = \sigma_1/\sigma_2$. Finally, both cavities are detuned by a factor $\delta = (\omega_2 - \omega_1)\tau_c$ for reasons that will become clear later. Let us suppose that only cavity 1 is pumped ($g_1 > 0$ and $g_2 < 0$). Therefore, cavity 2 acts as a saturable absorber cavity and hence s is necessarily much greater than 1 [19]. We take $s = 10$. The laser threshold for a single, uncoupled nanocavity is attained for $g_1 = N_1 = 1$. In order to derive a simple expression for the pump at laser threshold $g_1 = g_{\text{th}}$ of detuned coupled cavities, we take $g_2 = -1$ [20] and no coupling losses ($\gamma = 0$). The threshold can be found by solving

$$[\delta - \alpha(1 + g_{\text{th}})]^2 (g_{\text{th}} - 1) = \left[\frac{\kappa^2}{2} + (1 - g_{\text{th}})\right](3 - g_{\text{th}})^2.$$

If the coupling constant is small, we get $g_{\text{th}} \simeq 1 + 2\kappa^2/[(2\alpha - \delta)^2 + 4]$. The threshold naturally increases with κ because of the increased coupling of energy between the two cavities and has a maximum for $\delta = 2\alpha$ which corresponds to maximum energy transfer between the two cavities. This can be easily understood as one recalls that the phase-amplitude coupling term will progressively detune the cavities as pump increases. Detuned cavities are less coupled and thus the intensity needed to saturate the absorption in cavity 2 will increase. To counteract this effect and maintain a maximum coupling between the cavities when operating close to threshold, increasing saturation of the absorber in cavity 2, we introduce a detuning term $\delta \sim 2\alpha$.

Numerical simulations. The system of equations (1) is numerically investigated with the following parameters compatible with a semiconductor medium: $\gamma_r = 0.03$, $\kappa = 1$, $\gamma = 0$, $\alpha = 5$, $\delta = 10$, and $g_2 = -1$. These correspond to $\tau_c = 6$ ps and to a nonradiative recombination time of carriers of 200 ps. A bifurcation analysis [21] allows one to monitor the dynamics and its qualitative changes, as shown in Fig. 2. When the pump increases, the system starts to lase continuously at point B. Then the system undergoes a subcritical Hopf bifurcation (H1) at $g_1 \geqslant 1.60$, giving rise to high amplitude pulses. When the pump further increases, pulses become more and more nonlinear with a more complex envelope and a longer tail. Point D marks the end of stable self-pulsation and the system goes back to its cw steady state. Note that in that region the system is subcritical again and pulses disappear through a reverse Hopf (H2). In the self-pulsing region, the SP period τ_R varies with pumping between $40\tau_c$ and $65\tau_c$, i.e., between 240 and 400 ps, for pulses (a)–(d) in the inset of Fig. 2. At the same time, the pulse duration decreases by 25%. Thus, we predict pulses in the multi-GHz range with shortest durations around 35 ps.

We analyzed the dynamics for fixed pump $g_1 = 1.60$ in the (δ,κ) plane (Fig. 3). To do so, we integrate the dynamical equation (1) up to $5000\tau_c$, i.e., after a time range much longer than any relaxation time in the system, and record the maximum and minimum amplitude in a $1000\tau_c$-long integration interval. For a sizable range of values of the detuning δ and of the coupling constant κ, SP dynamics is found. For certain values of these parameters, a subcritical behavior is evidenced leading to bistability between a cw lower branch and a SP upper branch.

The dynamics is not always regular and chaos (Ch region in Fig. 3) can be found as a result of a series of period-doubling bifurcations. We have computed the maximum Lyapunov exponent of the dynamical system using [22]. Regions where one of the Lyapunov exponents is strictly greater than zero

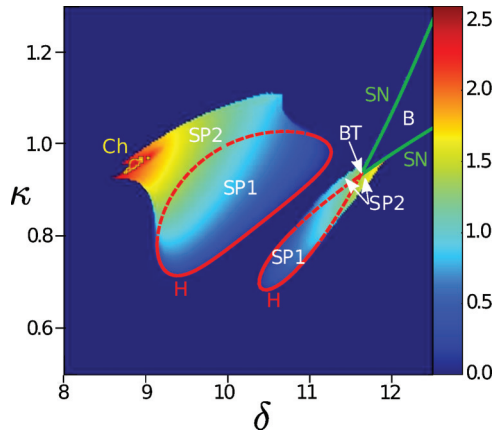

FIG. 3. (Color) Simplified bifurcation diagram in the (δ,κ) plane for $g_1 = 1.60$, superimposed to the maximum amplitude of the generated pulses. Saddle-node lines (SN) enclose a bistable region (B) between cw regimes; supercritical, periodic self-pulsing regions (SP1) are enclosed by Hopf bifurcation lines (H; continuous, supercritical; dashed, subcritical); (BT), Bogdanov-Takens point; zero amplitude regions correspond to cw lasing; SP2, periodic, subcritical self-pulsation. Region delimited by the yellow line is chaotic (Ch). Other parameters are the same as in Fig. 2.

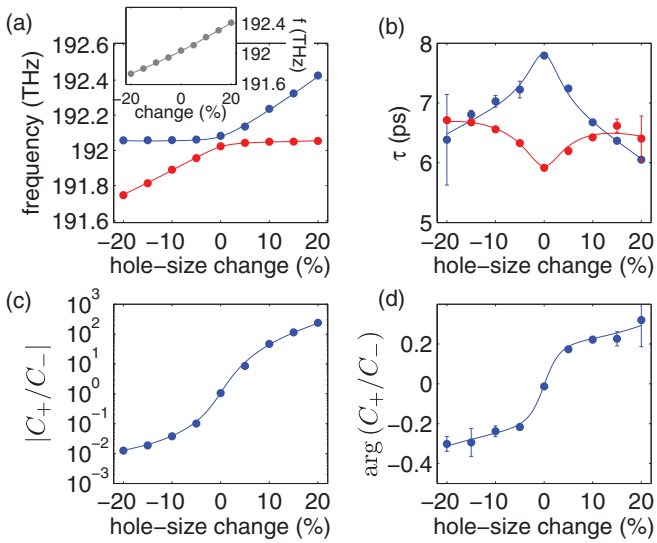

FIG. 4. (Color online) Resonant frequency (a), mode lifetime (b), amplitude ratio (c) and phase difference (d) for the bonding (blue, dark gray) and antibonding [red (light-gray)] modes versus hole-size change. Dots, 3D-FDTD simulations; lines, coupled-mode theory with parameters obtained from the inversion of Eqs. (3) and (4) and subsequent quadratic fits (see Fig. 5). Inset: single-cavity resonant frequency shift vs hole-size change, FDTD results (dots), and quadratic fit (line).

are enclosed in yellow in Fig. 3. This behavior occurs in the subcritical region, giving interesting prospects for switchable chaotic nanolaser sources. In the limit of very high coupling ($\kappa \gg 1$), we recover the SP scenario of the Yamada model, which describes a bisection laser with intracavity saturable absorber [23], giving the ability to attain the excitable regime [24]. In this model, SP occurs through a homoclinic bifurcation giving rise to pulses with an infinite period at threshold. Thus, we may expect that our scheme gives more robust pulses with respect to noise, and in particular, we expect less pulse to pulse jitter.

Experimental feasibility. Photonic crystals are ideal platforms to implement coupled nanocavity systems. We choose the paradigmatic L3 nanocavities as versatile and robust cavity geometry. Yet, we emphasize that the general concept presented above is not *a priori* restricted to a particular design. Standard cavity Q factors of the order of a few thousands are targeted as a good compromise between a low laser threshold and a short (picosecond) cavity lifetime [17]. Two adjacent PhC cavities are coupled by evanescent fields. The optical coupling strength depends on both the cavity separation and the coupling direction [25]. Carrier diffusion can be ignored in that case since the diffusion length is estimated to be $\sqrt{D_h/\gamma_r} \simeq 300$ nm for our typical semiconductor parameters, with $D_h = 5$ cm^2/s the hole diffusion constant [26], which is far below the intercavity distance $d = 1$ μm considered here. In the same spirit, thermal diffusion is characterized by a diffusion constant of the order of $D_{\rm th} = 0.33$ cm^2/s [27]. This means that the temperature reaches the same value in both cavities after a transient time $d^2/D_{\rm th} \simeq 30$ ns. Therefore our model remains valid within quasi-cw or cw pumping conditions.

In order to study regimes with coupling parameters close to 1 as in previous paragraphs, i.e., where the mode splitting is of the order of the resonance width, frequency splitting must be of the order of ~100 GHz. This regime is obtained for two L3 cavities aligned along the Γ-K direction and separated by three holes (see Fig. 1).

Our specific goal is to design a PhC coupled-cavity system with parameters compatible with the previous analysis. First, we show that we can tune the resonant frequency of a single L3 cavity by modifying two neighboring hole radii (see Fig. 1). We usethree-dimensional finite-difference time domain [28] (3D-FDTD) simulations together with a harmonic inversion algorithm [29] to recover all the cavity parameters (photon lifetime and losses) as a function of the hole radius change [Fig. 4(a), inset]. Next, we consider the transparent ($N_1 = N_2 = 0$) regime of model (1), which reads in its dimensional form

$$\frac{da_{1,2}}{dt} = i\Omega_{1,2}a_{1,2} + iKa_{2,1}, \qquad (2)$$

where $\Omega_{1,2} = \omega_{1,2} + i/\tau_{1,2}$ are the complex frequencies, $\tau_{1,2}$ are the cavity lifetimes, and $K = \tilde{\kappa} - i\tilde{\gamma}$ is the dimensional complex coupling constant. We consider two asymmetric coupled units in the linear regime to retrieve the cavity parameters of the coupled system. The left nanoresonator will play the role of the pumped unit (cavity 1), and the right resonator with the modified holes (cavity 2) will be the unpumped one. A large bandwidth dipole excitation is placed at the center of cavity 2 and we simulate by 3D-FDTD the evolution of the electric fields.

In terms of Eq. (2), this corresponds to the initial conditions $a_1(0) = 0$ and $a_2(0) = a_0$, where a_0 represents the excitation intensity. Equation (2) can be solved to give $a_2(t) = a_2(0)(C_+e^{i\Omega_+ t} + C_-e^{i\Omega_- t})$, where the plus and minus signs stand for bonding and antibonding modes, respectively; $C_\pm$ are given by the initial conditions and the eigenvalues

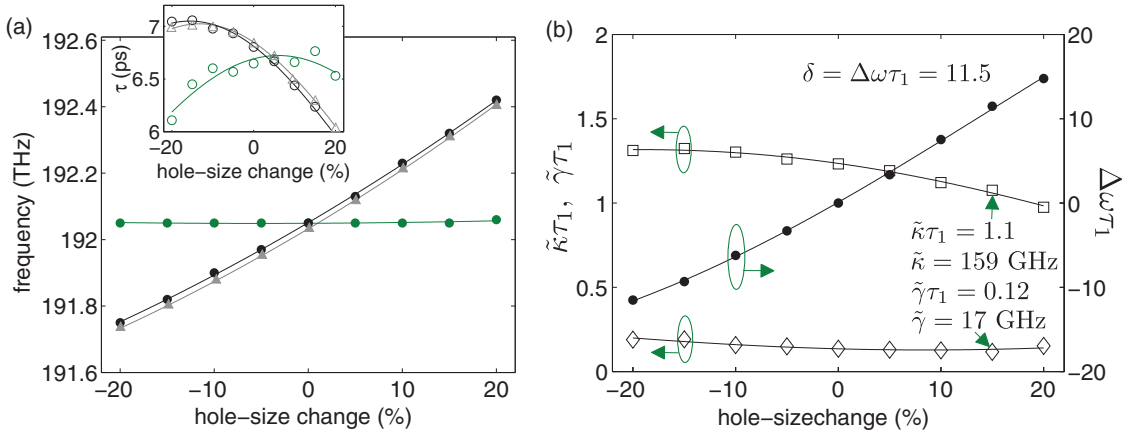

FIG. 5. (Color online) (a) Resonant frequencies of cavities 1 and 2 [respectively, green (light-gray) and black dots] obtained by inverting Eqs. (3) and (4) with FDTD simulation results. Gray triangles, single-cavity resonant frequency. Inset: mode lifetimes of cavities 1 and 2 [green (light-gray) and black open circles]; single-cavity lifetime (gray open triangles). (b) Imaginary (open squares) and real (open diamonds) coupling parameters obtained as in (a). Dots, normalized cavity detuning; lines, quadratic fits.

$\Omega_\pm = \omega_\pm + i/\tau_\pm$ yield

$$\Omega_\pm = \frac{\Omega_1 + \Omega_2 \pm \sqrt{(\Omega_1 + \Omega_2)^2 - 4(\Omega_1\Omega_2 - K^2)}}{2}, \quad (3)$$

$$C_+ = \frac{\Omega_+ - \omega_1 - i/\tau_1}{\Omega_+ - \Omega_-}, \qquad C_- = 1 - C_+. \quad (4)$$

In addition to the complex eigenfrequencies, the amplitude ratio and relative phase of the eigenmodes can be directly extracted from the FDTD simulations. The results are shown in Figs. 4(a)–4(d), evidencing anticrossing for the eigenfrequency curves, and loss splitting [30]. The six real parameters of Eq. (2) can thus be obtained by numerically inverting Eqs. (3) and (4). In order to get continuous model parameters, they are subsequently fitted with quadratic polynomials, as shown in Figs. 5(a) and 5(b). We observe that (i) the resonant frequencies of the coupled cavities are slightly blueshifted compared to those of the single cavity [31,32]; (ii) cavity 1 losses vary within ∼10% of the single-cavity losses due to the modification in cavity 2; (iii) the coupling constants slightly change as the cavities are detuned. Solutions of Eq. (3) with the inverted parameters of Fig. 5 are superimposed to the FDTD results [Figs. 4(a)–4(d)], showing that our simple coupled-mode approach can accurately capture the asymmetric PhC coupled-cavity system. Moreover, coupling constants κ of the order of 1 together with frequency detuning δ up to 10 can be realized. For 15% increase of hole size we obtain (see Fig. 5) parameters close to the target values for SP. Other coupling configurations [25] could be used to obtain much higher coupling constants, in particular, those allowing one to recover a homoclinic bifurcation at threshold.

Self-pulsing in real system. The real system introduced so far displays a nonzero real coupling coefficient γ. It also appears that both cavities have slightly different Q factors and for a +15% change in hole diameter the photon lifetime of cavity 1 is 6.8 ps and 6.3 ps for cavity 2. It is easy to introduce such difference in the original model (1). The complex coupling term is now $(i\kappa + \gamma) = 1.1i + 0.12$. Analysis of the bifurcation diagram shows that SP starts subcritically with high amplitude pulses at $g_1 \simeq 1.619$ with increasing pumping. We recover qualitatively the same behavior as shown previously, i.e., pulse amplitude increases and pulses become more and more nonlinear with a growing fat tail at the end of the pulse.

Conclusion. In conclusion, we have analyzed a model of semiconductor coupled-cavity nanolasers that revealed a rich dynamical scenario, showing the presence of SP and chaotic dynamics. For such dynamics to appear, we stress that it is necessary to detune one of the cavities to compensate for the phase-amplitude coupling term. The ability to tune the complex coupling coefficient in PhC coupled defect nanocavities has been used to design a system allowing the experimental observation of the predicted dynamics, and allows a great variety of coupling constants to be explored. Moreover, this system may be interesting in view of studying parity-time ($\mathcal{PT}$) symmetry breaking [33] in nanosystems.

Acknowledgments. We thank R. Kuszelewicz, F. Raineri, and A. Levenson for fruitful discussions and careful reading of the manuscript. The authors acknowledge partial support from the ANR Blanc project Optiroc.

[1] H. Altug, D. Englund, and J. Vuckovic, Nat. Phys. **2**, 484 (2006).
[2] F. Raineri, A. M. Yacomotti, T. J. Karle, R. Hostein, R. Braive, A. Beveratos, I. Sagnes, and R. Raj, Opt. Express **17**, 3165 (2009).
[3] R. Braive, S. Barbay, I. Sagnes, A. Miard, I. Robert-Philip, and A. Beveratos, Opt. Lett. **34**, 554 (2009).
[4] S. Matsuo, A. Shinya, T. Kakitsuka, K. Nozaki, T. Segawa, T. Sato, Y. Kawaguchi, and M. Notomi, Nat. Photon. **4**, 648 (2010).
[5] E. M. Purcell, Phys. Rev. **69**, 681 (1946).
[6] W.-H. Chang, W.-Y. Chen, H.-S. Chang, T.-P. Hsieh, J.-I. Chyi, and T.-M. Hsu, Phys. Rev. Lett. **96**, 117401 (2006).

[7] S. Strauf, N. G. Stoltz, M. T. Rakher, L. A. Coldren, P. M. Petroff, and D. Bouwmeester, Nat. Photon. **1**, 704 (2007).
[8] A. Armaroli, S. Malaguti, G. Bellanca, S. Trillo, A. de Rossi, and S. Combrié, Phys. Rev. A **84**, 053816 (2011).
[9] V. Grigoriev and F. Biancalana, Phys. Rev. A **83**, 043816 (2011).
[10] S. Malaguti, G. Bellanca, A. de Rossi, S. Combrié, and S. Trillo, Phys. Rev. A **83**, 051802 (2011).
[11] M. Heuck, S. Blaaberg, and J. Mørk, Opt. Express **18**, 18003 (2010).
[12] A. M. Yacomotti, P. Monnier, F. Raineri, B. B. Bakir, C. Seassal, R. Raj, and J. A. Levenson, Phys. Rev. Lett. **97**, 143904 (2006).
[13] M. Brunstein, A. M. Yacomotti, I. Sagnes, F. Raineri, L. Bigot, and A. Levenson, Phys. Rev. A **85**, 031803 (2012).
[14] T. Gu, N. Petrone, J. McMillan, A. van der Zande, M. Yu, G. Lo, D. Kwong, J. Hone, and C. Wong, Nat. Photon. **6**, 554 (2012).
[15] K. D. Chik, J. C. Dyment, and B. A. Richardson, J. Appl. Phys. **51**, 4029 (1980).
[16] S. Lim, J. Hudgings, G. Li, W. Yuen, K. Lau, and C. Chang-Hasnain, Electron. Lett. **33**, 1708 (1997).
[17] T. Yoshie, M. Loncar, A. Scherer, and Y. Qiu, Appl. Phys. Lett. **84**, 3543 (2004)
[18] M. Bache, F. Prati, G. Tissoni, R. Kheradmand, L. Lugiato, I. Protsenko, and M. Brambilla, Appl. Phys. B **81**, 913 (2005).
[19] This is due to the sublinear (usually taken as logarithmic) dependence of the gain on carrier density in quantum wells. It is worth noting that the actual value of the parameter s does not qualitatively change the results.
[20] Taking $\sigma_2 = 1 \times 10^{-16}$ cm^2, $\tilde{N}_0 = 1 \times 10^{18}$ cm^{-3}, $\Gamma = 0.2$, $\tau_c = 6$ ps, $n = 3.5$, and $P = 0$ we get $g_2 = -1.03$.
[21] Auto continuation software http://indy.cs.concordia.ca/auto/.
[22] M. Sandri, Math. J. **6**, 78 (1996).
[23] J. L. A. Dubbeldam and B. Krauskopf, Opt. Commun. **159**, 325 (1999).
[24] S. Barbay, R. Kuszelewicz, and A. M. Yacomotti, Opt. Lett. **36**, 4476 (2011).
[25] A. R. A. Chalcraft, S. Lam, B. D. Jones, D. Szymanski, R. Oulton, A. C. T. Thijssen, M. S. Skolnick, D. M. Whittaker, T. F. Krauss, and A. M. Fox, Opt. Express **19**, 5670 (2011).
[26] M. Brunstein, A. Yacomotti, R. Braive, S. Barbay, I. Sagnes, L. Bigot, L. Le-Gratiet, and J. Levenson, IEEE Photonics J. **2**, 642 (2010).
[27] M. Brunstein, R. Braive, R. Hostein, A. Beveratos, I. Rober-Philip, I. Sagnes, T. J. Karle, A. M. Yacomotti, J. A. Levenson, V. Moreau, G. Tessier, and Y. D. Wilde, Opt. Express **17**, 17118 (2009).
[28] J. D. Joannopoulos, S. G. Johnson, J. N. Winn, and R. D. Meade, *Photonic Crystals: Molding the Flow of Light*, 2nd ed. (Princeton University Press, Princeton, NJ, 2008).
[29] S. G. Johnson, Harmonic inversion software, http://ab-initio.mit.edu/wiki/index.php/Harminv.
[30] K. A. Atlasov, K. F. Karlsson, A. Rudra, B. Dwir, and E. Kapon, Opt. Express **16**, 16255 (2008).
[31] H. Erzgräber, S. Wieczorek, and B. Krauskopf, Phys. Rev. E **78**, 066201 (2008).
[32] R. Lang and A. Yariv, IEEE J. Quantum Electron. **24**, 66 (1988).
[33] C. E. Ruter, K. G. Makris, R. El-Ganainy, D. N. Christodoulides, M. Segev, and D. Kip, Nat. Phys. **6**, 192 (2010).